International Journal of Heat and Mass Transfer 52 (2009) 4812–4822

Contents lists available at ScienceDirect

International Journal of Heat and Mass Transfer

journal homepage: www.elsevier.com/locate/ijhmt

Effects of doping on the optical fiber drawing process

Chunming Chen, Yogesh Jaluria *

Department of Mechanical and Aerospace Engineering, Rutgers, The State University of New Jersey, Piscataway, NJ 08854, USA

ARTICLE INFO

Article history:
Received 30 January 2009
Received in revised form 16 May 2009
Accepted 16 May 2009
Available online 15 July 2009

Keywords:
Optical fiber drawing
Core-cladding structure
Zonal method
Glass radiation

ABSTRACT

Optical fibers are typically drawn from silica preforms, which usually consist of two concentric cylinders called the core and the cladding, heated in a high-temperature furnace. For optical communication purposes, the core generally has a higher average refractive index than the cladding to obtain total internal reflection. This paper investigates the effects of adding dopants to the core or to the cladding, to change the refractive index values, on the optical fiber drawing process. Employing an analytical/numerical model developed earlier to simulate the core-cladding structure of a typical optical fiber, the paper considers different dopants and the effects resulting from the consequent changes in properties, particularly the radiation absorption properties, on the temperature distributions, flow, neck-down profile, thermally induced defects and draw tension. The zonal method is applied to model the radiation transfer in the glass perform and the purge gas is taken as non-participating. The numerical model has been validated by comparing with results available in the literature, wherever possible. It is found that the effects are significant because of changes in refractive index and absorption of radiation, which give rise to significant changes in temperature and tension. These can, in turn, substantially affect fiber quality and characteristics. Therefore, for an accurate and realistic modeling of the process, the effects of property changes due to dopants on the draw process must be included.

1. Introduction

Silica glass (SiO_2) is the most common material used in optical fibers for telecommunication because of its low transmission loss. Besides silica, some other oxides called dopants are also employed to form optical fibers, which usually consist of two layers, the high-refractive-index core and the low-refractive index cladding. The refractive index profile is determined by the type and concentration of dopants. For example, GeO_2, P_2O_5, TiO_2, and Al_2O_3 are often used to increase the refractive index; F and B_2O_3 are used to reduce the refractive index. After doping, the refractive index of the core is usually slightly higher than that of the cladding by 0.1–1%. In practice, the maximum refractive index difference obtained for GeO_2, P_2O_5, B_2O_3 and F are 3.5%, 1.2%, −0.5% and −0.7%, respectively. Any larger amounts of dopants added to silica would cause failure in vitrification and result in cracks in the glass during the drawing due to the thermal expansion mismatch between the dopants and silica [1].

The major purpose of doping is to obtain a desirable refractive index profile in the optical fiber. However, doping also significantly changes other properties of the material, such as the absorption coefficient and the viscosity [2]. For example, the addition of GeO_2 to pure silica increases its absorption coefficient and lowers its viscosity. The variation in these two properties may have considerable effect on the temperature field, the neck-down profile and the applied draw tension, which are crucial to the optical fiber drawing process. Therefore, it is important to include the effects of doping in the numerical simulation of the optical fiber drawing process.

Although many experimental studies have been carried on the optical fiber drawing process with a variety of dopants, there is not much simulation effort devoted to this problem [1,2], mainly because of the complexity of the problem. Yin [3] briefly investigated the effect of using a double-layer cylinder on the temperature field. Only the effect of change in the refractive index and the absorption coefficients was studied. However, the information provided by Yin [3] is not very helpful in understanding the effect of doping on optical fiber drawing because the physical properties of doped silica were not included in his study and radiation transport in a cylinder is very different from that in a realistic neck-down profile. Therefore a more rigorous model for double-layer fiber drawing process is needed to study the effect of dopants.

In this paper, only step index fibers are considered. Each of the core and the cladding is assumed to have a uniform refractive index and absorption coefficient. Both the interface and the free surface are assumed to be diffuse. Non-diffuse surfaces can also be considered if accurate property data on the surface are available. The zonal method is applied to calculate the axial and radial transport by thermal radiation in the glass. A fully conjugate analysis, involving the flows in the core, the cladding and the purge gas, has been carried out. Three widely used dopants are considered here, GeO_2 as the core dopant and B_2O_3 and F as the cladding

* Corresponding author. Tel.: +1 732 445 3652; fax: +1 732 445 4021.
E-mail address: jaluria@jove.rutgers.edu (Y. Jaluria).

0017-9310/$ - see front matter © 2009 Elsevier Ltd. All rights reserved.
doi:10.1016/j.ijheatmasstransfer.2009.05.021

Nomenclature

a	absorption coefficient
C_p	specific heat at constant pressure
D	diameter
E	activation energy
F_T	draw tension
K	thermal conductivity
L	preform length
n	refractive index; defect concentration
p	pressure
r, z	radial and axial coordinates
R	radius
S_r	radiation source term
T	temperature
t	time
u, v	radial and axial velocity components

Greek symbols

χ	mole fraction in%
λ	wavelength
μ	dynamic viscosity
υ	kinematic viscosity
σ	density
Φ	viscous dissipation term

Subscripts

0	preform inlet
c	centerline
d	defect
F	furnace
f	fiber
lag	difference between center and surface values
melt	glass softening point

Superscripts

(1)	core
(2)	cladding
(3)	gas

dopants. In order to obtain useful insight into the optical fiber drawing process, the physical properties of doped silica are obtained by best fits to the data available in the literature. Finally, the effect of dopants on the optical fiber drawing process and the concentration of E' defects are investigated.

2. Analysis

2.1. Estimation of properties

In order to investigate the effects of dopants on optical fiber drawing, the optical, thermal and mechanical properties of doped silica have to be obtained as the first step. Among these properties, surface tension, specific heat, and thermal conductivity have been found to change very little for the small amount of dopants added to pure silica, as seen from data in the references given earlier. Thus, they are obtained from the measurements for pure silica.

The radiative properties, including the refractive index and the absorption coefficient, are strongly dependent on the type and the concentration of the dopants. Fig. 1 shows the variation of the refractive index with the dopant concentration for various dopants [1]. It can be seen that the relationship between the change in refractive index and dopant concentration is linear for GeO_2, B_2O_3, and F. Thus, the relationship can be approximated as,

$$\Delta = c \cdot \chi, \tag{1}$$

where χ is the mole fraction in% and Δ is the difference in refractive index n between doped and pure silica, given as,

$$\Delta = \frac{n^{(1)} - n^{(2)}}{n^{(1)}}. \tag{2}$$

For Fig. 1, c is estimated to be 0.0902 for GeO_2-doped silica, -0.069 for B_2O_3-doped silica and -0.4479 for F.

The three-band model is obtained by best fits to Izawa and Sudo's data [4] for pure silica, 6.0 mole% GeO_2-doped silica, and 4.3 mole% B_2O_3-doped silica. Obviously, other best fits are possible, particular if interest lies in particular wavelength λ ranges, such as small values. For pure fused silica with low OH content, the band absorption model in terms of the absorption coefficient a is

$$a = 0, \quad \text{for } \lambda < 0.15\ \mu\text{m}, \tag{3}$$

$$a = 0.0059\ \text{cm}^{-1}, \quad \text{for } 0.15\ \mu\text{m} \leqslant \lambda < 3.0\ \mu\text{m}, \tag{4}$$

$$a = 0.8455\ \text{cm}^{-1}, \quad \text{for } 3.0\ \mu\text{m} \leqslant \lambda < 4.8\ \mu\text{m}, \tag{5}$$

$$a = 345.0\ \text{cm}^{-1}, \quad \text{for } 4.8\ \mu\text{m} \leqslant \lambda < 8.0\ \mu\text{m}. \tag{6}$$

For 6.0 mole% GeO_2-doped silica, the model is

$$a = 0, \quad \text{for } \lambda < 0.15\ \mu\text{m}, \tag{7}$$

$$a = 0.0445\ \text{cm}^{-1}, \quad \text{for } 0.15\ \mu\text{m} \leqslant \lambda < 3.0\ \mu\text{m}, \tag{8}$$

$$a = 0.8455\ \text{cm}^{-1}, \quad \text{for } 3.0\ \mu\text{m} \leqslant \lambda < 4.8\ \mu\text{m}, \tag{9}$$

$$a = 345.0\ \text{cm}^{-1}, \quad \text{for } 4.8\ \mu\text{m} \leqslant \lambda < 8.0\ \mu\text{m}. \tag{10}$$

Since GeO_2 has a similar atomic structure as compared to silica, and the infrared absorption spectra of 6.0 mole% GeO_2-doped silica is found to be almost the same as pure silica [4], the absorption coefficients in the wavelength region $3.0\ \mu\text{m} \leqslant \lambda < 4.8\ \mu\text{m}$ are assumed to be independent of the GeO_2 concentration. In the ultraviolet region, the absorption coefficient increases in proportion to the GeO_2 concentration and the absorption coefficient is given as [4]

$$A_{UV} = 1542\Delta/(446\Delta + 6000) \times 10^2 \exp(4.63/\lambda) \quad (\text{dB/km}). \tag{11}$$

From Eqs. (1), (7), and (10), the absorption coefficient for GeO_2-doped silica in the wavelength region $0.15\ \mu\text{m} \leqslant \lambda < 3.0\ \mu\text{m}$ can be expressed as a function of refractive index difference Δ as,

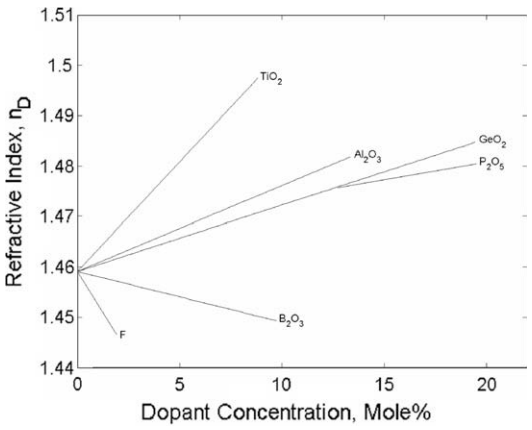

Fig. 1. Refractive index of common dopants for silica (adapted from Murata [1]).

$$a(\Delta) = \frac{513.195\Delta}{446\Delta + 6000}\ \mathrm{cm}^{-1}. \quad (12)$$

For 4.3 mole% B_2O_3-doped silica,

$$a = 0, \quad \text{for } \lambda < 0.15\ \mu\mathrm{m}, \quad (13)$$

$$a = 0.0192\ \mathrm{cm}^{-1}, \quad \text{for } 0.15\ \mu\mathrm{m} \leqslant \lambda < 3.0\ \mu\mathrm{m}, \quad (14)$$

$$a = 1.466\ \mathrm{cm}^{-1}, \quad \text{for } 3.0\ \mu\mathrm{m} \leqslant \lambda < 4.8\ \mu\mathrm{m}, \quad (15)$$

$$a = 759.0\ \mathrm{cm}^{-1}, \quad \text{for } 4.8\ \mu\mathrm{m} \leqslant \lambda < 8.0\ \mu\mathrm{m}. \quad (16)$$

In the case of B_2O_3-doped silica, the two strongest absorption bands are the B–O band at 7.9 μm and the Si–O band at 9.1 μm. The intensities of these two bands are determined by the concentration of B_2O_3. The B–O band at 7.9 μm becomes stronger and shifts to shorter wavelength with increasing B_2O_3 concentration, as do the absorption coefficients in the wavelength region $\lambda < 8.0$ μm [4,5]. Because of lack of data in the available literature for various B_2O_3 concentrations, the absorption coefficients for B_2O_3-doped silica are assumed to be in proportion to the B_2O_3 concentration in this paper.

Addition of F into silica extends the transmission of silica into shorter wavelengths [6]. Thus the F-doped silica may have higher transmission in that region than pure silica. A small amount of F doping is usually needed due to its strong effect on refractive index, as shown in Fig. 1. Therefore, the absorption coefficient of F-doped silica is approximated as that of pure silica.

The density of pure silica can be taken as a constant, at an approximate value of 2200.0 kg/m^3. The density for GeO_2- and B_2O_3-doped silica is obtained by curve-fitting of experimental data [1], given as the following:

$$\rho(\Delta) = 0.0059\Delta^2 + 159.9753\Delta + 2199.0374, \quad \text{for } GeO_2\text{-doped silica}, \quad (17)$$

$$\rho(\Delta) = 0.2189\Delta^2 + 73.8588\Delta + 2201.3979, \quad \text{for } B_2O_3\text{-doped silica}. \quad (18)$$

The kinematic viscosity υ of pure silica in SI units is taken from Fleming [7] as

$$\upsilon(T) = 4545.5 \exp\left[32\left(\frac{T_{\mathrm{melt}}}{T} - 1\right)\right], \quad (19)$$

The viscosity μ of GeO_2-doped silica is given by Tajima et al. [8] as follows,

$$\mu(T, \Delta) = \mu_0(T) \exp(-A\Delta), \quad (20)$$

where the decrement coefficient $A = 0.5$ for these data; $\mu_0(T)$ is the viscosity of pure silica, and Δ is the refractive index difference between the GeO_2-doped silica and pure silica. Although this equation was obtained for a small change in refractive index with GeO_2 doping ($\Delta < 0.58$), Tajima et al. [8] showed that it might still be valid for GeO_2-doped preform with larger amount of dopants. At a temperature of 1973.15 K, the decrement coefficient A is found to be 0.55 for the viscosity of pure GeO_2 glass ($\Delta = 10$), which has only a 10% difference from that used in Eq. (20).

The viscosity of B_2O_3-doped silica can be expressed as [1],

$$\mu(T, \Delta) = \mu_0(T)\left[\exp\left(\frac{c_1(\Delta)}{T} + c_2(\Delta)\right)\right], \quad (21)$$

Table 1
Parameters of Eq. (21) for the viscosity of B_2O_3-doped silica.

Composition (mole% B_2O_3)	Refractive index difference Δ (%)	c_1	c_2
6.2	−0.4278	52981.9323	−15.6062
10.1	−0.6969	46652.3890	−13.8806
14.6	−1.0074	41936.9838	−13.1744

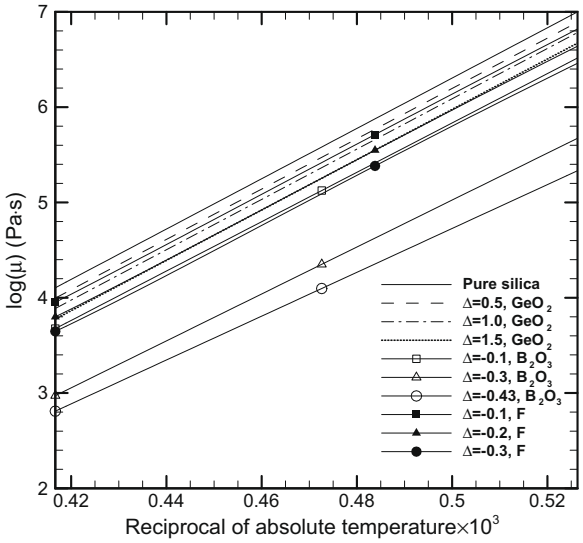

Fig. 2. Relationship between viscosity and temperature for pure silica and doped silica.

where μ_0 is the viscosity of pure silica and Δ is the refractive index difference between the B_2O_3-doped silica and pure silica. After curve-fitting of the experimental data from Urbain et al. [9], $c_1(\Delta)$ and $c_2(\Delta)$ are obtained and given in Table 1. The viscosity of F-doped silica is taken from Ohashi et al. [10] and given as,

$$\mu(T, \Delta) = \mu_0(T) \exp[(-13.5129t^4 + 82.0376t^3 - 174.4330t^2 + 145.1302t - 28.8756)\Delta], \quad (22)$$

where $t = 0.001 \times (T - 273.15)$.

From Eqs. (19)–(22), the relationships between the logarithmic values of viscosity and temperature for pure silica and doped silica are shown in Fig. 2. It is clear that, when silica is doped with GeO_2, B_2O_3, and F, the viscosity significantly decreases with increasing doping, being most strongly affected by B_2O_3.

2.2. Governing equations

The governing equations derived in earlier papers [11,12] are used in this paper. The flows in the glass and the gas are assumed to be laminar and axisymmetric, due to the low mass flow rates. The buoyancy effect is neglected since it has been shown in earlier papers to be negligible for most practical circumstances. Since the density of the glass does not change much during the drawing process and the speed of the gas is low, the flows of the glass and the gas can be treated as incompressible. Therefore the governing equations for glass and gas are given as,

$$\frac{\partial v}{\partial z} + \frac{1}{r}\frac{\partial (ru)}{\partial r} = 0, \quad (23)$$

$$\frac{\partial v}{\partial t} + u\frac{\partial v}{\partial r} + v\frac{\partial v}{\partial z} = -\frac{1}{\rho}\frac{\partial p}{\partial z} + \frac{1}{r}\frac{\partial}{\partial r}\left[r\upsilon\left(\frac{\partial u}{\partial z} + \frac{\partial v}{\partial r}\right)\right] + 2\frac{\partial}{\partial z}\left(\upsilon\frac{\partial v}{\partial z}\right), \quad (24)$$

$$\frac{\partial u}{\partial t} + u\frac{\partial u}{\partial r} + v\frac{\partial u}{\partial z} = -\frac{1}{\rho}\frac{\partial p}{\partial r} + \frac{2}{r}\frac{\partial}{\partial r}\left(r\upsilon\frac{\partial u}{\partial r}\right) + \frac{\partial}{\partial z}\left[\upsilon\left(\frac{\partial u}{\partial z} + \frac{\partial v}{\partial r}\right)\right] - \frac{2\upsilon u}{r^2}, \quad (25)$$

$$\rho C_p\left(\frac{\partial T}{\partial t} + u\frac{\partial T}{\partial r} + v\frac{\partial T}{\partial z}\right) = \frac{1}{r}\frac{\partial}{\partial r}\left(rK\frac{\partial T}{\partial r}\right) + \frac{\partial}{\partial z}\left(K\frac{\partial T}{\partial z}\right) + \Phi + S_r, \quad (26)$$

where Φ is the viscous dissipation term given as,

$$\Phi = \mu\left\{2\left[(\frac{\partial u}{\partial r})^2 + \left(\frac{u}{r}\right)^2 + \left(\frac{\partial v}{\partial z}\right)^2\right] + \left(\frac{\partial u}{\partial z} + \frac{\partial v}{\partial r}\right)^2\right\}, \quad (27)$$

and S_r is the radiation source term. In these equations, u, v are the velocity components along coordinates r and z, t is time, T is temperature, K is thermal conductivity and C_p is the specific heat at constant pressure. Both the viscous dissipation term and the radiation source term can be neglected for the gas. That is due to the fact that the viscosity of the gas is small and the gas can be considered to be non-participating. However, convection in the gas is very important, particularly near the end of the neck-down region, and must be considered. In the presented results, the furnace radius is denoted by R_F, the perform radius by R_0 and the fiber radius at the exit by $R^{(2)}$. The furnace length is denoted by L and the softening point of glass as T_{melt}.

The stream function and vorticity equations are solved instead of continuity and momentum equations. Thus the pressure does not need to be solved simultaneously and one equation is eliminated, leading to a simpler numerical scheme and faster convergence for the axisymmetric problem considered. The complex domains for the core, the cladding and the purge gas are converted to cylindrical regions. The zonal method is applied to simulate the radiation transport in the neck-down profile. The boundary conditions are similar to those given in cited papers, which may be consulted for further details. Dopant diffusion is negligible, compared to the convection effects. For the exit boundary conditions, the axial diffusion terms are set equal to zero. Symmetry is used at the axis and no-slip conditions are used at the surface. Continuity of temperature, velocity, heat flux and shear across the interface are employed.

2.3. Method of solution

Body-fitted grid systems are generated for the domains of the core, the cladding, and the inert gas based on the method proposed by Lee and Jaluria [13] and Yin and Jaluria [14]. Two grid sets are applied here. Both of these are non-uniform. A fine grid system is used to discretize the stream function, Vorticity, and temperature equations. The coarse grid system is applied to the radiation analysis. After optimization, the grids are obtained as 369×21 (in z- and r-directions, respectively) for the core, 369×21 for the cladding and 369×61 for the gas. Coarser grids are obtained for radiation, 31×9 for the core and 31×11 for the cladding. The radiative heat fluxes absorbed by axisymmetric volume ring elements within the preform are first calculated by the zonal method using the coarse grid system and then interpolated to obtain the radiative source terms at the fine grid for the energy equation. Since computation of the direct exchange areas for the zonal method is very time-consuming, a parallelization for this computation is developed with the Message-Passing Interface (MPI).

The stream function and vorticity equations are solved instead of continuity and momentum equations. Thus the pressure does not need to be solved simultaneously and one equation is eliminated, leading to a simpler numerical scheme and faster convergence for the axisymmetric problem considered. The complex domains for the core, the cladding and the purge gas are converted to cylindrical regions. The zonal method is applied to simulate the radiation transport in the neck-down profile. The boundary conditions are similar to those given in cited papers, which may be consulted for further details. Dopant diffusion is negligible, compared to the convection effects. For the exit boundary conditions, the axial diffusion terms are set equal to zero. Symmetry is used at the axis and no-slip conditions are used at the surface. Continuity of temperature, velocity, heat flux and shear across the interface are employed.

3. Results and discussion

In order to investigate the effect of dopants on optical fiber drawing, four kinds of combinations of dopants are considered: GeO_2-doped silica core with a pure silica cladding, pure silica core with B_2O_3-doped silica cladding, pure silica core with F-doped silica cladding, and GeO_2-doped silica core with F-doped silica cladding. In this paper, the diameters of the preform and the fiber are taken at typical values of 5 cm and 125 μm, respectively. Other values can similarly be considered for a given system. The ratio of diameters of the core and the preform is set at a typical value of 1:2. Radiation transport at the end of the finite-sized furnace is considered in terms of the iris, opening and moving fiber [12]. The diameter of the furnace is taken as 7 cm and the temperature distribution for the furnace is taken as [13],

$$T_F = 2500 - 2000\left(\frac{z}{L} - 0.5\right)^2. \quad (28)$$

The preform is pulled at a draw speed of 10 m/s and the temperature of the preform in the inlet is taken as 300 K. Argon is the working fluid for aiding flow, which enters the furnace at a speed of 0.1 m/s and a temperature of 300 K. These conditions are fixed at these typical values, since the effects of variations in these have been considered earlier.

3.1. Effect of doping in the core

GeO_2 is mainly used as dopant for the core to increase the refractive index, which will also increase the ultra-violet radiation absorption and lower the viscosity. In this study, the core is doped with 5.5 mole%, 11.1 mole%, and 16.6 mole% GeO_2, respectively, to obtain a relative refractive index difference of 0.5%, 1.0%, and 1.5% in the fiber. The physical properties of GeO_2-doped silica are given in Table 2.

In Fig. 3, the isotherms for various GeO_2 concentrations are shown with a reference profile to demonstrate the variations in temperature levels in the axial direction. It is seen that, when the core is doped with GeO_2, the core is heated up to the same temperature level in a shorter distance than the cladding. The distance to reach a certain temperature level for the whole preform decreases

Table 2
Estimated properties of GeO_2-doped silica.

Refractive index difference Δ (%)	0.5	1	1.5
Composition mole (%)	5.5432	11.0865	16.6297
Density (kg/m^3)	2279.0265	2359.0186	2439.0136
Absorption coefficient	$a = 0$, for $\lambda < 0.15$ μm $a = 0.0412$ cm^{-1}, for 0.15 μm $\leqslant \lambda < 3.0$ μm $a = 0.8455$ cm^{-1}, for 3.0 μm $\leqslant \lambda < 4.8$ μm $a = 345.0$ cm^{-1}, for 4.8 μm $\leqslant \lambda < 8.0$ μm	$a = 0$, for $\lambda < 0.15$ μm $a = 0.0796$ cm^{-1}, for 0.15 μm $\leqslant \lambda < 3.0$ μm $a = 0.8455$ cm^{-1}, for 3.0 μm $\leqslant \lambda < 4.8$ μm $a = 345.0$ cm^{-1}, for 4.8 μm $\leqslant \lambda < 8.0$ μm	$a = 0$, for $\lambda < 0.15$ μm $a = 0.1154$ cm^{-1}, for 0.15 μm $\leqslant \lambda < 3.0$ μm $a = 0.8455$ cm^{-1}, for 3.0 μm $\leqslant \lambda < 4.8$ μm $a = 345.0$ cm^{-1}, for 4.8 μm $\leqslant \lambda < 8.0$ μm
Viscosity (Pa s)	$\mu_0(T)\exp(-0.25)$	$\mu_0(T)\exp(-0.5)$	$\mu_0(T)\exp(-0.75)$

with increasing GeO_2 concentration. The reason is that, since GeO_2-doped silica core has larger radiation coefficient in the ultra-violet region and the transmissivity of pure silica cladding is very high in this region, the GeO_2-doped silica core absorbs more energy by radiation than pure silica core. Fig. 4 shows the temperature of the preform along the centerline for pure silica and GeO_2-doped silica core with a pure silica cladding, for various GeO_2 concentrations. As expected, a significant increase in the centerline temperature is observed in the upper neck-down region with greater GeO_2 doping. Beyond that, the fiber with higher GeO_2 concentration maintains a slightly higher temperature along the centerline.

The temperature lag, defined as $T_{lag} = (T_s - T_c)/T_c$, indicating the temperature difference from the core, for the free surface, is shown in Fig. 5. The peak lag along the free surface occurs very close to the entrance and is followed by the minimum lag. The magnitudes of the peak and minimum lag are strongly affected by GeO_2 doping due to higher temperature levels in the core. When GeO_2 concentration goes up to 16.6 mole%, the peak lag decrease from 0.33 to 0.05 and the minimum lag also goes down from 0 to −0.07. GeO_2 doping also influences the temperature lag along the inner interface. For pure silica, the temperature along inner interface is found to be higher than that at the centerline since the radiation heat flux decreases exponentially in the radial direction. For GeO_2-doped silica core with pure silica cladding fiber, the temperature along the inner interface is found to be lower than that along the centerline and the minimum lag decreases with an increase of GeO_2 concentration as expected.

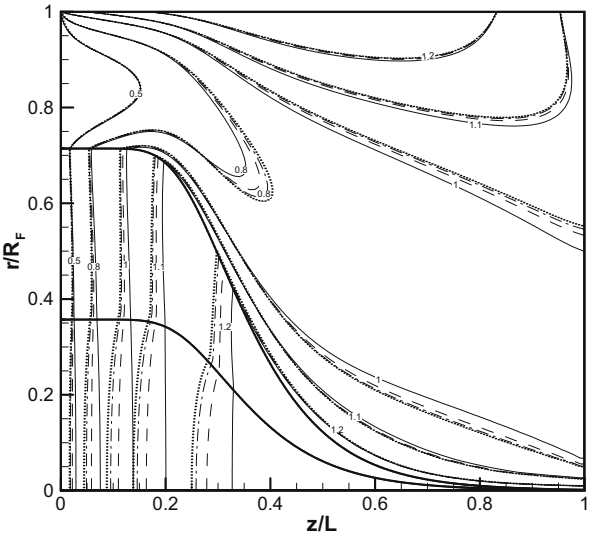

Fig. 3. Isotherm for various GeO_2 concentrations (solid line: pure silica; dashed line: 5.5 mole% GeO_2; dashed dot line: 11.1 mole% GeO_2; dotted line: 16.6 mole% GeO_2).

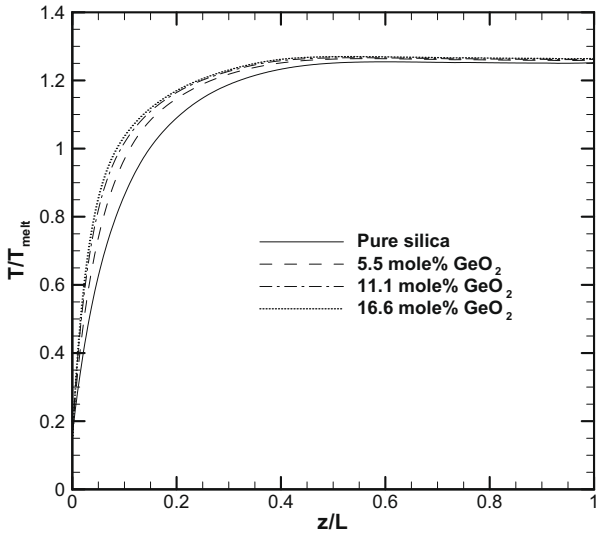

Fig. 4. Temperature variation along the centerline for various GeO_2 concentrations.

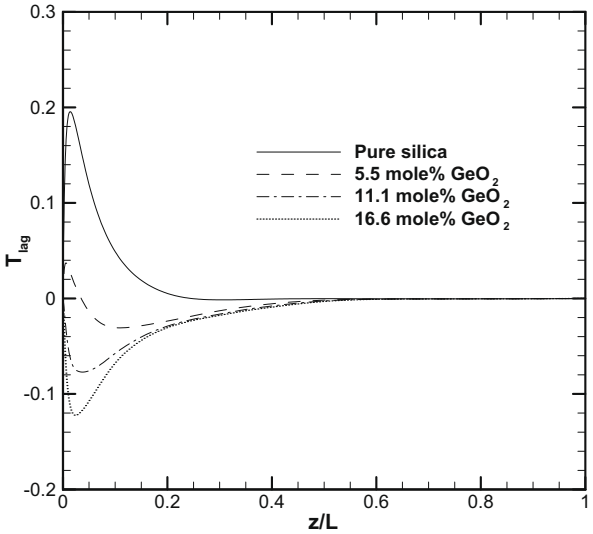

Fig. 5. Temperature lag along the free surface for various GeO_2 concentrations.

The E' defect is a point defect, which is generated at high temperature during the drawing process and which causes transmission loss and mechanical strength degradation in the fiber [18]. The equation for E' defect concentration is given as [19],

$$\nu \frac{dn_d}{dz} = n_p(0)\,\nu \exp\left(-\frac{E_p}{KT}\right) - n_d\,\nu\left[\exp\left(-\frac{E_p}{KT}\right) + \exp\left(-\frac{E_d}{KT}\right)\right], \tag{29}$$

where n_d and E_d represent the concentration and activation energy of the E' defect; n_p and E_p represent those of the precursors. The initial values and constants are defined as [18], $n_d(0) = 0$, $n_p(0) = 7 \times 10^{22}\ g^{-1}$, $E_p = 6.4087 \times 10^{-19}$ J, $E_d = 0.3204 \times 10^{-19}$ J, $\nu = 8 \times 10^{-3}\ s^{-1}$, and $K = 1.380658 \times 10^{-23}$ J/K.

Normalized concentration of E' defects, which are drawing-induced and generated at high temperature, is shown in Fig. 6 along the centerline. It is seen that the E' defects are mainly generated in the upper neck-down region, while the temperature undergoes a drastic increase. As expected, the concentration of E' defects increases with increasing GeO_2 concentration because of higher preform temperature. Since the core undergoes a history of higher temperature, the concentration of E' defects in the core at the exit is found to be significantly higher than that in the cladding. As expected, the concentration of E' defects was found to be larger in the double-layer preform due to higher preform temperature. It was found that the fiber quality is degraded with an increase in refractive index difference between the core and the cladding in term of E' defects.

Fig. 7 shows the effect of GeO_2 doping on the neck-down profile. It is seen that the neck-down profile is steeper for larger GeO_2 concentration. The reason for this is that viscosity of GeO_2-doped silica core decreases with increasing GeO_2 concentration, as shown in

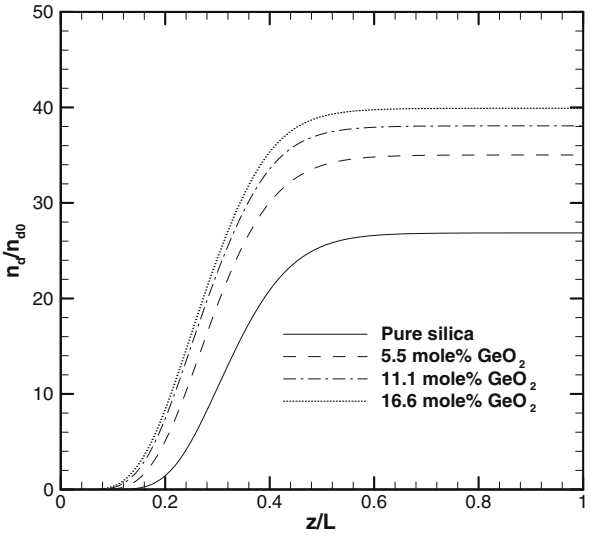

Fig. 6. Concentration of E' defects along the centerline for various GeO_2 concentrations.

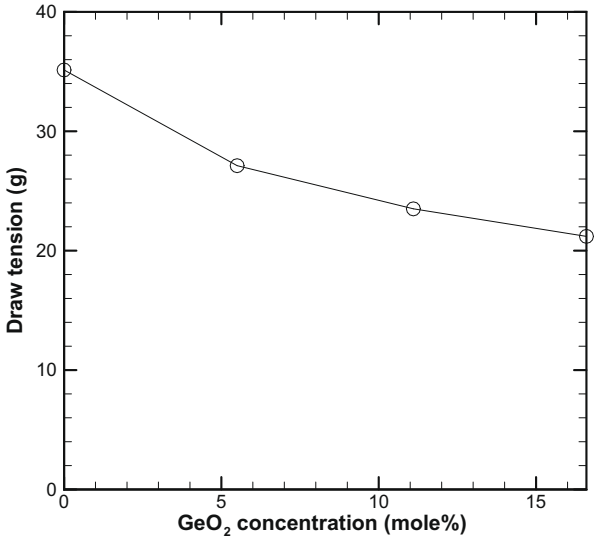

Fig. 8. Draw tension for various GeO_2 concentrations.

Fig. 2, and higher preform temperature due to radiation also causes further decrease in the viscosity of the fiber. Fig. 8 shows that the draw tension decreases with increasing GeO_2 concentration. Experimental results by Tajima et al. [8] showed a linear relation between the draw tension and relative refractive index difference in a GeO_2-doped silica fiber drawing process with $\Delta < 0.3$. However, the numerical results for larger amount of GeO_2 doping ($\Delta < 1.5$) suggest a nonlinear relationship between the draw tension and the GeO_2 concentration. After curve-fitting the results in Fig. 8 with a third-order polynomial, the relationship is given in gram force as,

$$F_T = -4.1254\chi^3 + 14.9985\chi^2 - 22.5058\chi + 35.1354 \quad (\mathrm{g}). \qquad (30)$$

3.2. Effect of doping in the cladding

In order to study the effect of doping in the cladding, B_2O_3 and F are used as cladding dopants to obtain a relative refractive index difference up to 0.43% and 0.3%, respectively. Incorporation of either of these two dopants into silica would also cause lower viscosity and larger absorption coefficients for B_2O_3-doped silica, while the absorption spectra of F-doped silica are assumed to be unchanged from pure silica. The physical properties of B_2O_3-doped silica and F-doped silica are shown in Fig. 2 and Table 3.

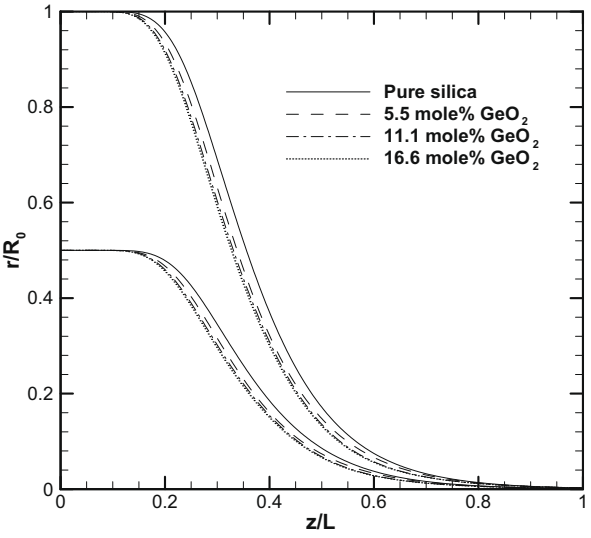

Fig. 7. Neck-down profiles for various GeO_2 concentrations.

Fig. 9 shows the isotherms for pure silica core with B_2O_3-doped cladding preform as a reference profile. It is seen that in the near-entrance region, the preform doped with B_2O_3 is heated up to the same temperature level in a shorter distance than pure silica, beyond that it takes a longer distance to do so. The reason for this is that, when the cladding is doped with B_2O_3, the cladding is heated up by radiation faster in the near-entrance region. However, less radiative heat flux passes through the cladding and the high temperature along the free surface also increases the energy loss to purge gas due to convection, which eventually causes a lower preform temperature than pure silica preform. The effect of B_2O_3 doping on the temperature variation along the centerline is shown in Fig. 10. As expected, comparing with pure silica preform, the centerline temperature for pure silica core with B_2O_3-doped cladding preform is slightly higher in the upper neck-down region and becomes lower beyond that. The temperature lags along the free surface and inner interface were also calculated. It was found that the peak of temperature lag along the free surface and inner interface occurs near the entrance and increases with increasing B_2O_3 concentration. A decrease in the minimum lag along the free surface is also found, which may be due to convection cooling.

The concentration of E' defects along the centerline, inner interface and free surface were determined, as shown in Fig. 11 for the variation along the centerline. The concentration of E' defects decrease with increasing B_2O_3 concentration because of lower preform temperature in the neck-down region. It is also interesting to observe that the change in concentration of E' defects becomes very small when B_2O_3 concentration is larger than 4.3 mole%. The concentration of E' defects at the exit was found to be almost uniform, indicating the core and cladding undergo a similar temperature history.

The effect of B_2O_3 concentration on the neck-down profile is shown in Fig. 12. It is seen that the neck-down profile becomes steeper with B_2O_3 concentration less than 4.3 mole% and does not change much beyond that. The reason may be that when B_2O_3 concentration is less than 4.3 mole%, viscosity of B_2O_3-doped silica cladding drastically decreases with increasing B_2O_3 concentration, despite the preform temperature being low. When B_2O_3 concentration is larger than 4.3 mole%, viscosity of B_2O_3-doped sil-

Table 3
Estimated properties of B_2O_3-doped silica.

Refractive index difference Δ (%)	−0.1	−0.3	−0.4278
Composition mole (%)	1.4493	4.3478	6.2
Density (kg/m^3)	2194.0142	2179.26	2169.8412
Absorption coefficient	a = 0, for $\lambda < 0.15$ μm a = 0.009 cm^{-1}, for 0.15 μm $\leqslant \lambda <$ 3.0 μm a = 0.9905 cm^{-1}, for 3.0 μm $\leqslant \lambda <$ 4.8 μm a = 441.7742 cm^{-1}, for 4.8 μm $\leqslant \lambda <$ 8.0 μm	a = 0, for $\lambda < 0.15$ μm a = 0.0152 cm^{-1}, for 0.15 μm $\leqslant \lambda <$ 3.0 μm a = 1.2806 cm^{-1} for 3.0 μm $\leqslant \lambda <$ 4.8 μm a = 635.3226 cm^{-1}, for 4.8 μm $\leqslant \lambda <$ 8.0 μm	a = 0, for $\lambda < 0.15$ μm a = 0.0192 cm^{-1}, for 0.15 μm $\leqslant \lambda <$ 3.0 μm a = 1.466 cm^{-1}, for 3.0 μm $\leqslant \lambda <$ 4.8 μm a = 759.0 cm^{-1}, for 4.8 μm $\leqslant \lambda <$ 8.0 μm
Viscosity (Pa s)	$\exp\left(\frac{c_1(\Delta)}{T}+c_2(\Delta)\right)$ where, c_1 = 59644.7627, c_2 = −16.3882	$\exp(\frac{c_1(\Delta)}{T}+c_2(\Delta))$ where, c_1 = 56717.3463, c_2 = −16.788	$\exp(\frac{c_1(\Delta)}{T}+c_2(\Delta))$ where, c_1 = 52981.9323, c_2 = −15.6062

ica is so small compared to that of pure silica that the effective change in B_2O_3 concentration on the neck-down profile is negligible.

Fig. 13 shows the relation between the B_2O_3 concentration and draw tension. As expected, when B_2O_3 concentration is less than 4.3 mole%, the draw tension decreases with increasing B_2O_3 concentration, and draw tension does not change much beyond that. Based on the data in Fig. 13, a third-polynomial equation may be fitted to the results,

$$F_T = -1245.0\chi^3 + 985.0\chi^2 + 260.5\chi + 35.1 \quad \text{(g)}. \tag{31}$$

The isotherms for pure silica preform and pure silica core with F-doped silica cladding preform are shown in Fig. 14. As expected, the addition of F into the cladding has a minor effect

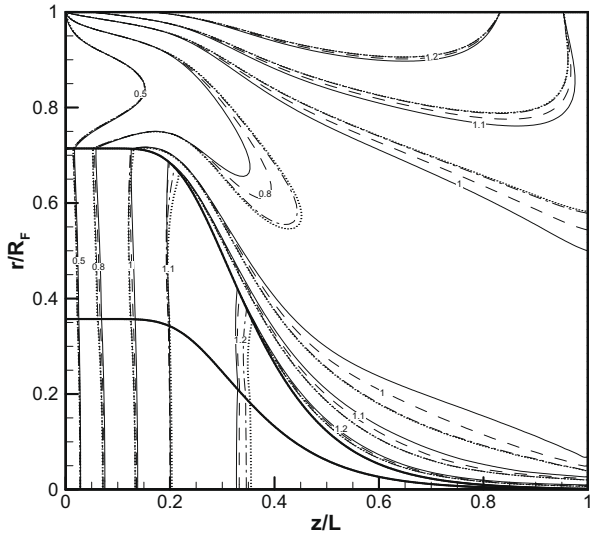

Fig. 9. Isotherm for various B_2O_3 concentrations (solid line: pure silica; dashed line: 1.4 mole% B_2O_3; dashed dot line: 4.3 mole% B_2O_3; dotted line: 6.2 mole% B_2O_3).

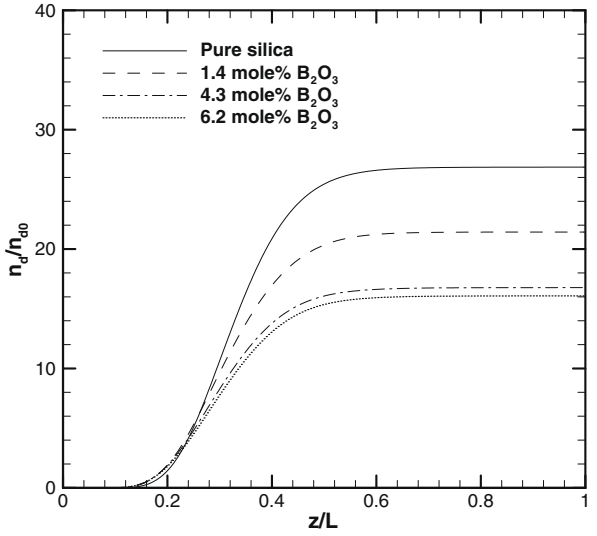

Fig. 11. Concentration of E' defects along the centerline for various B_2O_3 concentrations.

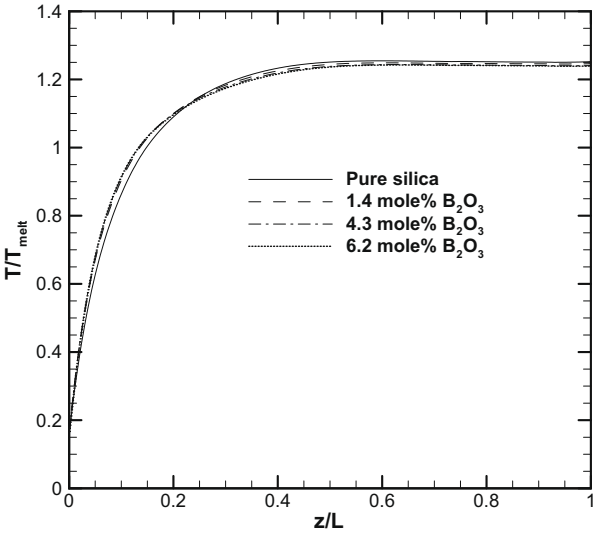

Fig. 10. Temperature variation along centerline for various B_2O_3 concentrations.

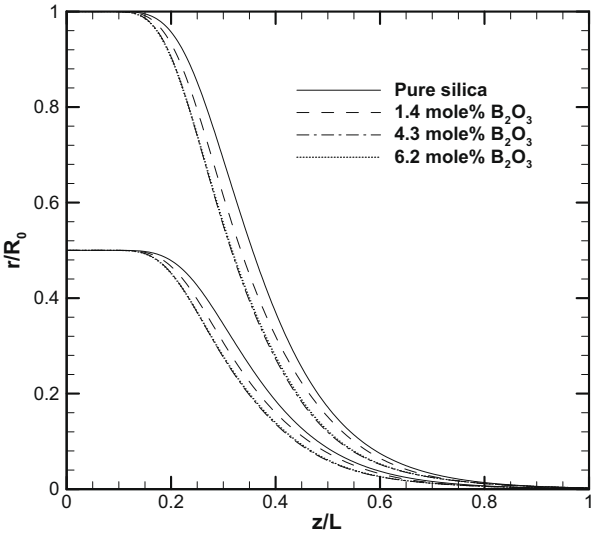

Fig. 12. Neck-down profile for various B_2O_3 concentrations.

on the temperature distribution in the preform. The normalized concentration of E' defects along the centerline, the free surface and inner interface were determined. It was found that the generation of E' defects in the lower neck-down decreases with increasing F concentration. This is mainly due to the fact that the preform temperature with F concentration is slightly lower than pure silica. The concentration of E' defects at the exit was found to be almost uniform.

The effect of F content on the neck-down profiles is shown in Fig. 15. It is clear that the diameter of the neck-down profile decreases with increasing F concentration due to lower viscosity of F-doped silica cladding. As expected, smaller draw tension is obtained for larger F concentration, as shown in Fig. 16. After curve-fitting against the results in Fig. 16, the relation between draw tension and F concentration is given as,

$$F_T = 377.0559\chi^3 - 100.8885\chi^2 - 58.1617\chi + 35.1354 \quad (\mathrm{g}). \tag{32}$$

A comparison between the results with B_2O_3 content and those with F content shows that, for the same level of relative refractive index, the effect of B_2O_3 content on fiber drawing process is stronger than that of F content. Lower E' defects' concentration and lower draw tension are obtained for B_2O_3 doping, which is desired for improving fiber quality. However, B_2O_3 content also causes larger residual stress due to larger viscosity difference between the core and the cladding, which would increase the transmission loss in the fiber [20].

3.3. Combined effect of doping in both core and cladding

In this study, GeO_2 is added into the core and F is used as a cladding dopant. In order to investigate the combined effect of doping in core and cladding, the relative refractive index difference between the core and the cladding remains as 1% ($\Delta^{(1)} - \Delta^{(2)} = 1\%$), while ratio of concentrations F/GeO_2 varies. The relative refractive index in the core ($\Delta^{(1)}\%$) varies from 1% to 0.7% by GeO_2 doping,

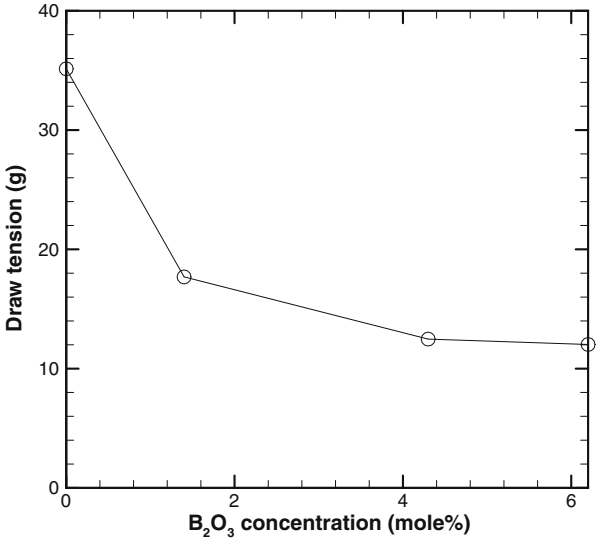

Fig. 13. Draw tension for various B_2O_3 concentrations.

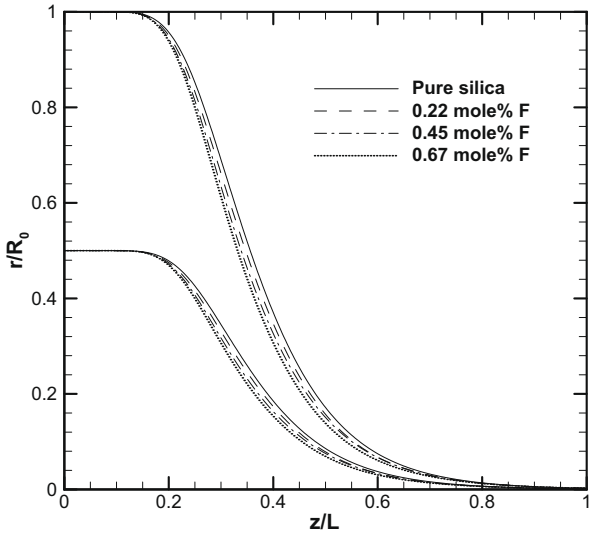

Fig. 15. Neck-down profiles for various F concentrations.

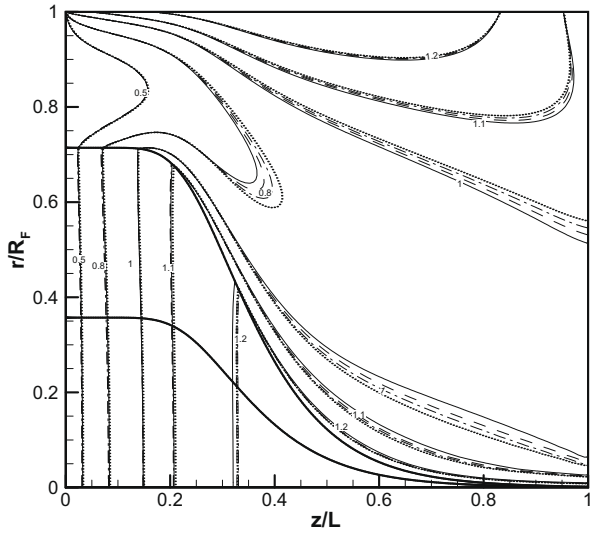

Fig. 14. Isotherm for various F concentrations (solid line: pure silica; dashed line: 0.22 mole% F; dashed dot line: 0.45 mole% F; dotted line: 0.67 mole% F).

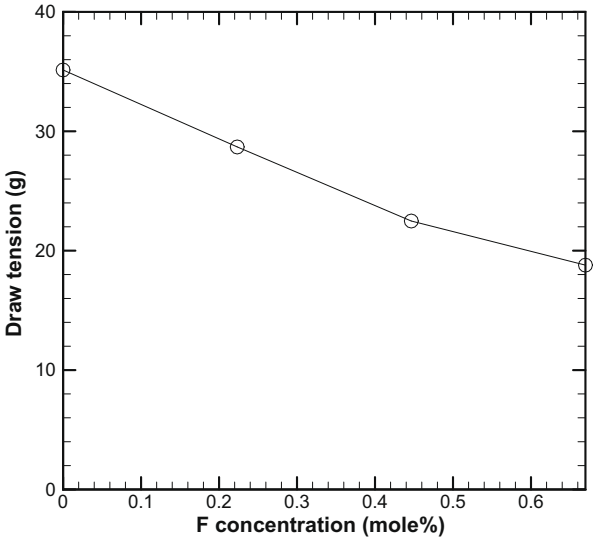

Fig. 16. Draw tension for various F concentrations.

and that in the cladding ($\Delta^{(2)}\%$) decreases from 0% to −0.3% by F doping.

As discussed earlier, F content has little effect on temperature distribution and GeO_2 content significantly increases the absorption in the core. Fig. 17(a) shows a similar pattern of isotherms as that with GeO_2-doped silica core with pure silica cladding preform. The core reaches the same temperature level in longer distance than the cladding, and the preform temperature decreases with increasing ratio of concentrations F/GeO_2. This is because absorption in the core decreases with decreasing GeO_2 concentration. As expected, both the peak lag and the minimum lag were found to increase with increasing ratio of concentrations F/GeO_2.

Fig. 17(b) shows the effect of ratio of concentrations F/GeO_2 on the concentration of E' defects at the exit. The concentration of E' defects in the core is higher than that in the cladding, which is similar to the results for GeO_2 content discussed earlier. However, a larger decrease in the concentration of E' defects is found with an increase in ratio of concentrations F/GeO_2, which indicates the combined effect of both dopants.

Since viscosity of silica is more strongly affected by F than GeO_2, the neck-down profile becomes steeper for larger ratio of concentrations F/GeO_2, as shown in Fig. 18(a). Fig. 18(b) shows the combined effect of GeO_2 and F on draw tension. The draw tension decreases with increasing ratio of concentrations F/GeO_2 as expected. Higher furnace temperatures reduce the tension, but also shorten the life of the furnace. After curve-fitting the results in Fig. 18(b), the relation is expressed as,

$$F_T = -1.7423\left(\frac{\chi_F}{\chi_{GeO_2}}\right)^3 + 7.502\left(\frac{\chi_F}{\chi_{GeO_2}}\right)^2 - 13.2908\left(\frac{\chi_F}{\chi_{GeO_2}}\right) + 23.5027 \quad (g). \tag{33}$$

3.4. Effect of draw speed and feasible drawing conditions

The effect of draw speed on the concentration of E' defects and draw tension for a GeO_2-doped silica core with pure silica cladding preform is investigated. Two draw speeds of 10 m/s and 20 m/s are considered.

Fig. 19(a) shows the concentration of E' defects at the exit. It is seen that when draw speed change from 10 m/s to 20 m/s, the concentration of E' defects decreases and the difference between the

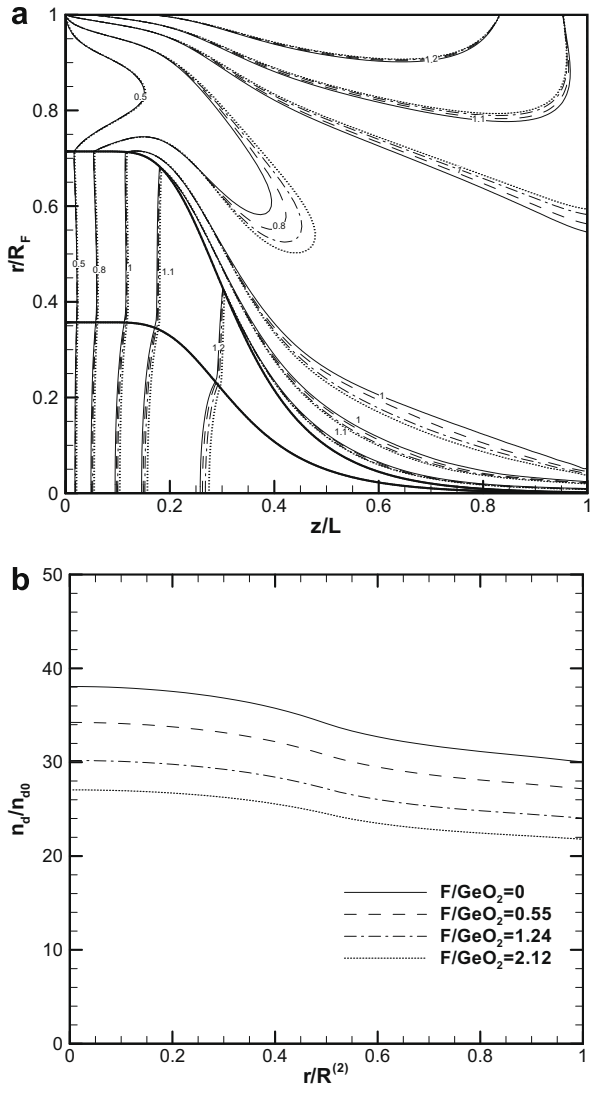

Fig. 17. (a) Isotherm for various ratios F/GeO_2 of the concentrations (solid line: pure silica; dashed line: $F/GeO_2 = 0.55$; dashed dot line: $F/GeO_2 = 1.24$; dotted line: $F/GeO_2 = 2.12$). (b) Concentration of E' defects at the exit for various ratios F/GeO_2.

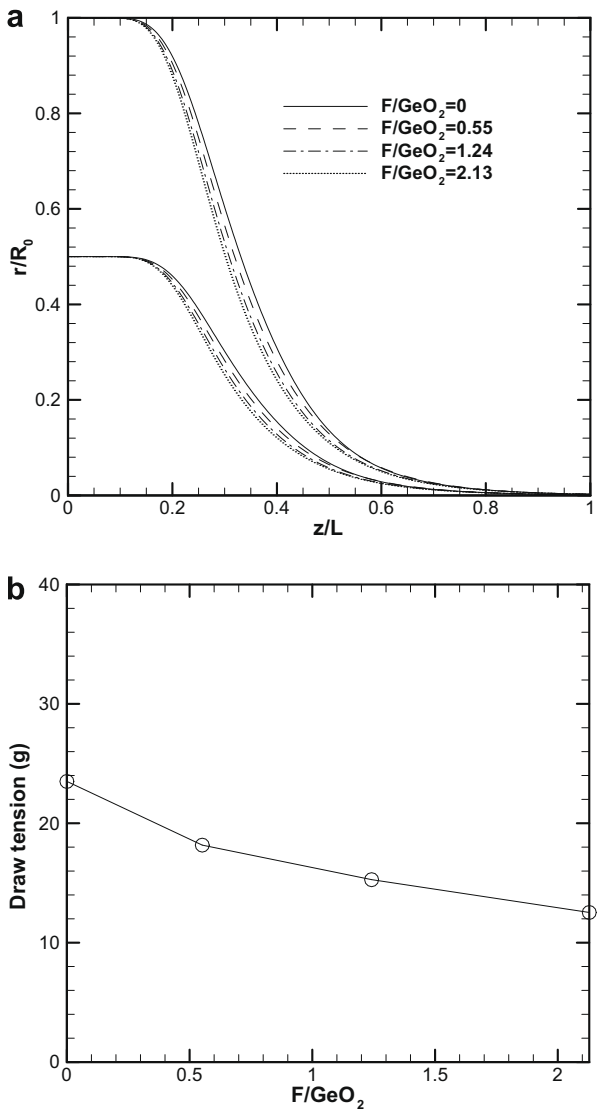

Fig. 18. (a) Neck-down profile for various ratios F/GeO_2 of the concentrations. (b) Draw tension for various ratios F/GeO_2.

core and the cladding increases. The reason for this is that the preform temperature is higher for lower draw speed.

Fig. 19(b) shows the draw tension for two draw speeds of 10 m/s and 20 m/s. It is seen that when the draw tension goes up to 20 m/s, the draw tension increases tremendously and the effect of change in GeO_2 concentration on draw tension become much stronger. The curve-fitting equation for draw speed of 20 m/s is given as,

$$F_T = -0.0164\chi^3 + 0.6360\chi^2 - 9.2219\chi + 105.6577 \quad (g). \qquad (34)$$

The comparison between the results for two draw speeds indicates that the preform undergoes a history of lower temperature and requires a higher draw tension when the draw speed goes up. In practice, a high draw speed is desired in order to increase the fiber productivity. However, for the given operation conditions such as furnace dimensions, furnace temperature, furnace length and draw-down ratio, a maximum draw speed exists. Beyond this limit, the preform will not reach the softening point, resulting in viscous rupture due to large viscosity. For a GeO_2-doped silica core with pure silica cladding preform, the maximum draw speed is expected to increase with increasing GeO_2 concentration because higher preform temperature is obtained. It is worthy to note that the preform can also be overheated to cause capillary instability when the draw speed is low with high furnace temperature or long furnace length. This minimum draw speed will increase as well with an increase in GeO_2 concentration.

For pure silica core with B_2O_3- or F-doped silica cladding preforms, the preform temperature decreases with increasing doping in the cladding. Therefore, the maximum allowed draw speed would be smaller for larger amount of doping in the cladding. For GeO_2-doped silica core with F-doped silica cladding preform, when ratio of concentrations F/GeO_2 increases, the maximum allowed draw speed decreases due to the lower preform temperature.

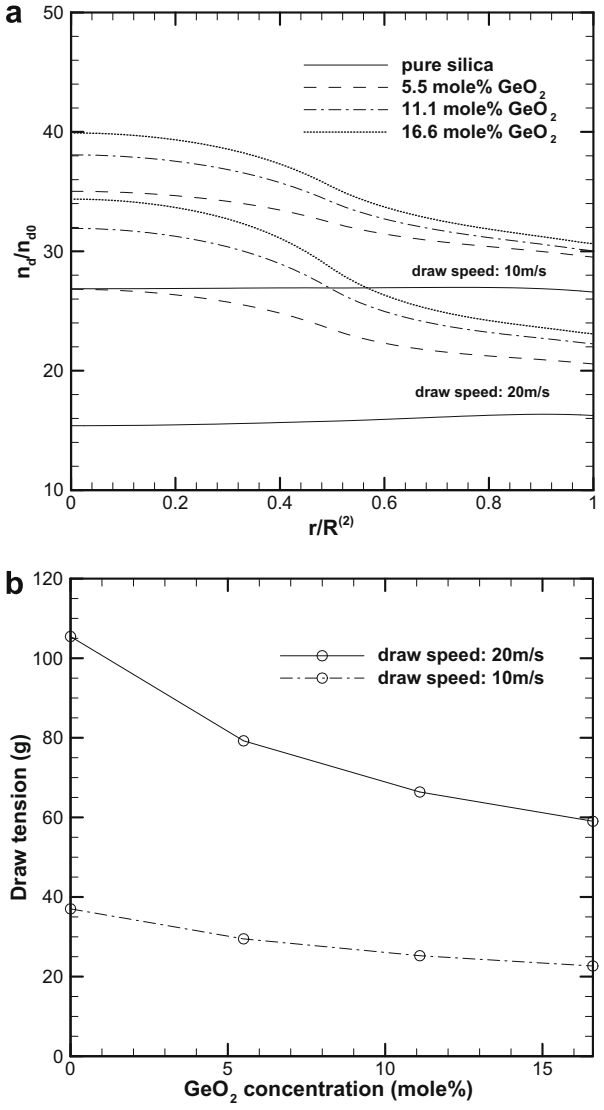

Fig. 19. (a) Concentration of E' defects for different draw speeds. (b) Draw tension for different draw speeds.

4. Conclusions

In this paper, the effect of doping on the optical fiber drawing is investigated in detail. First, GeO_2 is used as a core dopant to increase silica's refractive index with pure silica cladding having a low-refractive index. It is seen that the temperature in the core significantly increases with increasing GeO_2 concentration, which is higher than the temperature in the cladding. Thus the concentration of E' defects is highly non-uniform in the cross-section, larger in the core and smaller in the cladding. It is also found that the draw tension decreases almost linearly with an increase in GeO_2 concentration.

In order to investigate the effect of doping in the cladding, either B_2O_3 or F is added into the cladding to reduce the refractive index. For pure silica core with B_2O_3-doped silica cladding fiber, B_2O_3-doped silica cladding has larger absorption coefficients and lower transmissivity, which lead to a higher temperature level near the entrance and lower temperature level beyond that comparing with pure silica preform. When small amount of B_2O_3 (<4.3 mole%) are doped, the draw tension and concentration of E' defects decrease drastically with increasing B_2O_3 concentration and do not change much beyond that. For pure silica core with F-doped silica cladding fiber, the concentration of F has little effect on the temperature distribution. However, the concentration of E' defects and draw tension decreases with increasing F concentration due to the fact that F-doped silica has lower viscosity. Comparing with F, larger amount of B_2O_3 is needed to obtain the same refractive index difference, which also leads to smaller concentration of E' defects and draw tension.

After this, we considered the case when the core is doped with GeO_2 and the cladding is doped with F. The combined effect of these two dopants on the temperature distribution is similar to that of GeO_2. The concentration of E' defects decreases with increasing ratio of concentrations F/GeO_2. The relation between the draw tension and the ratio of concentrations F/GeO_2 is found to be linear. The effect of draw speed on GeO_2-doped silica core with pure silica cladding fiber drawing process is investigated. It is found that when the draw speed increases, the concentration of E' defects becomes smaller due to a lower preform temperature, and much larger draw tension is obtained. Thus, it is shown that the dopants affect the properties, resulting in a significant effect on the temperature field and hence on the draw tension and defects. These results will be valuable to industry and to future research on the draw process.

References

[1] H. Murata, Handbook of Optical Fibers and Cables, second ed., Marcel Dekker, New York, 1996.
[2] N.P. Bansal, R.H. Doremus, Handbook of Glass Properties, Academic Press, New York, 1986.
[3] Z. Yin, Numerical Investigation of Thermal Transport in Optical Fiber Drawing Processes, Ph.D. Thesis, Rutgers University, New Brunswick, NJ, 1997.
[4] T. Izawa, S. Sudo, Optical Fibers: Materials and Fabrication, KTK Scientific Publishers, Tokyo, 1987.
[5] J. Wong, C.A. Angell, Glass: Structure by Spectroscopy, Marcel Dekker, New York, 1976.

[6] C.M. Smith, L.A. Moore, Formation of absorption bands in f-doped silica under excimer laser exposure, SPIE 4346 (2001) 1080–1087.
[7] J.D. Fleming, Fused Silica Manual, Final Report for the US Atomic Energy Commission, Oak Ridge, Tennessee, Project No. B-153, 1964.
[8] K. Tajima, M. Tateda, M. Ohashi, Viscosity of GeO_2-doped silica glasses, J. Lightwave Technol. 12 (1994) 411–414.
[9] G. Urbain, F. Millon, S. Cariset, Viscosities of some silica rich liquids in the system SiO_2–B_2O_3, C.R. Hebd. Seances Acad. Sci. C290 (198) 137.
[10] M. Ohashi, M. Tateda, K. Tajima, K. Shiraki, Fluorine concentration dependence of viscosity in F-doped silica glass, Electron. Lett. 28 (1992) 1008–1010.
[11] C. Chen, Y. Jaluria, Modeling of radiation heat transfer in the drawing of an optical fiber with multi-layer structure, ASME J. Heat Transfer 129 (2007) 342–352.
[12] C. Chen, Y. Jaluria, Numerical simulation of transport in optical fiber drawing with core-cladding structure, ASME J. Heat Transfer 129 (2007) 559–567.
[13] S.H.K. Lee, Y. Jaluria, Effects of variable properties and viscous dissipation during optical fiber drawing, ASME J. Heat Transfer 118 (1996) 350–358.
[14] Z. Yin, Y. Jaluria, Thermal transport and flow in high-speed optical fiber drawing, ASME J. Heat Transfer 120 (1998) 916–930.
[15] Y. Jaluria, K.E. Torrance, Computational Heat Transfer, second ed., Taylor & Francis, New York, 2003.
[16] Y. Yan, R. Pitchumani, Numerical study on the dopant concentration and refractive index profile evolution in an optical fiber manufacturing process, Int. J. Heat Mass Transfer 49 (2006) 2097–2112.
[17] H. Huang, R.M. Miura, J.J. Wylie, Optical fiber drawing and dopant transport, SIAM J. Appl. Math. 69 (2008) 330–347.
[18] H. Hanafusa, Y. Hibino, F. Yamamoto, Formation mechanism of drawing-induced E' centers in silica optical fibers, J. Appl. Phys. 58 (1985) 1356–1361.
[19] Z. Yin, Y. Jaluria, Neck down and thermally induced defects in high speed optical fiber drawing, ASME J. Heat Transfer 122 (2000) 351–362.
[20] M. Ohashi, M. Tateda, K. Shiraki, K. Tajima, Imperfection loss reduction in viscosity-matched optical fibers, IEEE Photon. Technol. Lett.. 5 (1993) 812–814.